Supporting Information

Bechtel et al. 10.1073/pnas.1400502111

SI Text

Spectral Irradiance of Scattering-Scanning Near-Field Optical Microscopy IR Sources. Fig. 1*A* of the main text shows spectral irradiance curves for IR scattering-scanning near-field optical microscopy (*s*-SNOM) broadband sources. For the OPO (1) and supercontinuum (2) laser sources, the spectral irradiance was calculated using the published spectral profiles and total power of the source, assuming a diffraction-limited spot size achieved with a parabolic mirror with N.A. = 0.4. For the blackbody source, the spectral irradiance was calculated using a source temperature of 1,000 K [identical to Huth et al. (3)] with 90% IR emission efficiency, assuming emission into a 4π solid angle that is collected with a 0.4 N.A. IR lens with no other losses. Because the irradiance at the focus cannot exceed the irradiance at the source for spatially incoherent light, this is the upper limit for irradiance in a near-field experiment with a thermal source.

The spectral curve of the synchrotron source was measured via FTIR using the same instrumentation described above by placing a gold mirror in front of the atomic force microscope (AFM). The integrated power between 700 and 5,000 cm^{-1} was measured with a thermal power meter and an appropriately coated Ge filter. As with the laser sources, the diffraction-limited spot size was calculated using a focusing optic with N.A. = 0.4. The theoretical performance of Advanced Light Source (ALS) Beamline 5.4 was simulated with Synchrotron Radiation Workshop (SRW) (4) using the ALS synchrotron ring parameters and a beamline opening angle of 17×69 mrad vertical and horizontal, respectively. The simulation accounts for the 20 mirrors (98% reflectivity) between the source and the AFM tip, Fresnel reflection losses off the diamond window separating ultrahigh vacuum of the storage ring and the rough vacuum of the transport line, and the extended source of the bend magnet radiation, which reduces the collection efficiency by $\sim 1/2$ in this case. These calculations indicate that with an alternate detector–beamsplitter combination, synchrotron infrared nanospectroscopy (SINS) measurements could be extended to both lower (terahertz) and higher (near-IR) frequencies.

Instrument Response. Large dielectric constants allow metallic AFM tips to act as effective near-field scattering sources throughout the IR. As shown in Fig. S2*A*, strong signals are observed through the mid-IR regions with the greatest near-field signal enhancement being observed at low frequencies, compared with the far-field instrumental response spectrum. Although tip-to-tip variations have been observed, this result is reproducible among the platinum-coated silicon and platinum silicide tips used in these experiments and is expected from dielectric damping within a conducting tip. The near-field spectrum was recorded on a gold substrate, and the far-field spectrum was acquired by placing a flat, gold mirror in front of the AFM. These spectra are equivalent to "single-beam" spectra in conventional FTIR and are used to correct for the instrumental response of the system, including the source, beam-

splitter, and detector. In both cases, the spectral response at the low-frequency end is limited by the mercury cadmium telluride (MCT) detector, which has a cutoff at 700 cm^{-1}, and at the high-frequency end by both the MCT detector and KBr beamsplitter.

Spatio-Spectral Imaging. Figs. 3 and 4 show linescans obtained via the point-map method, in which spectra are averaged at an individual point for 10–300 s, depending on the signal-to-noise ratio and spectral resolution desired. For the model systems presented here and for many applications, one-dimensional line maps provide sufficient spatially resolved chemical information. For those applications that do require full 2D spatio-spectral imaging, area maps can also be measured using this same point-map method, a technique that is commonly used in far-field imaging as well. However, the time required for area mapping is significantly increased because of the unfavorable multidimensional scaling.

We have also devised an alternative mode of spatio-spectral imaging that takes advantage of the rapid-scan commercial interferometer and enables spectrally resolved 2D images at line rates of 0.1 Hz. This method has the ability to acquire about 40 spectra at 32-cm^{-1} spectral resolution per line simultaneously with the AFM topography. This real-time spectral imaging is particularly well-suited for samples having large signals and broad spectral features. However, even at 32-cm^{-1} spectral resolution, many key spectral features can be identified and used to locate regions of interest before higher spectral resolution measurements are performed with the point-map method. For samples with weaker signals, the image can be oversampled, such that multiple lines can be averaged together for improved signal-to-noise ratios.

Protein Measurements. Fig. S3 shows SINS spectra of two different dried proteins, BSA and γ-globulin, demonstrating the difference in lineshape and peak positions in the fingerprint region. In this case, we plot the imaginary component of the SINS referenced signal $\mathrm{Im}[\sigma_n/\sigma_{n,ref}]$, rather than the spectral phase $\Phi_n - \Phi_{n,ref}$, as in the main text. Both the imaginary and phase components of the *s*-SNOM signal approximate the absorption coefficient measured in traditional FTIR measurements (1, 2, 5). Thus, both can be used for direct mode assignment based on the peak maximum and lineshape. With increasing oscillator strength, however, the spectral phase approximation breaks down, and a small blue shift of several cm^{-1} occurs relative to the absorption coefficient, as observed in the Amide I modes shown in the main text. For the two protein spectra presented here, the SINS imaginary component matches the far-field peak positions exactly. To extract the exact real and imaginary components of the material dielectric constant, however, models of the tip polarizability must be considered, as described in detail elsewhere (5, 6).

1. Xu XG, Rang M, Craig IM, Raschke MB (2012) Pushing the sample-size limit of infrared vibrational nanospectroscopy: From monolayer toward single molecule sensitivity. *J Phys Chem Lett* 3:1836–1841.
2. Huth F, et al. (2012) Nano-FTIR absorption spectroscopy of molecular fingerprints at 20 nm spatial resolution. *Nano Lett* 12(8):3973–3978.
3. Huth F, Schnell M, Wittborn J, Ocelic N, Hillenbrand R (2011) Infrared-spectroscopic nanoimaging with a thermal source. *Nat Mater* 10(5):352–356.
4. Chubar O, Elleaume P (1998) Accurate and efficient computation of synchrotron radiation in the near field region. *Proceedings of the EPAC98 Conference* (IOP Publishing, Bristol, UK), pp 1177–1179.
5. Govyadinov AA, Amenabar I, Huth F, Carney PS, Hillenbrand R (2013) Quantitative measurement of local infrared absorption and dielectric function with tip-enhanced near-field microscopy. *J Phys Chem Lett* 4:1526–1531.
6. McLeod AS, et al. (2013) Model for quantitative near-field spectroscopy and the extraction of nanoscale-resolved optical constants. arXiv:1308.1784.
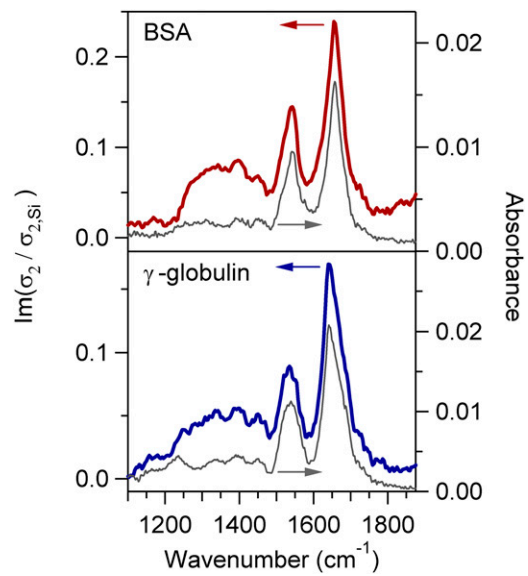
Fig. S1. Experimental schematic of the SINS experiment.

Fig. S2. Near-field (blue) and far-field (*Inset*, black) $|A(\bar{\nu})|$ spectra illustrating the instrumental response on gold. The features labeled with * originate from the diamond window that separates the ultrahigh vacuum of the synchrotron storage ring from the rest of the beamline. The feature labeled with † is associated with the MCT detector.

Bechtel et al. www.pnas.org/cgi/content/short/1400502111

2 of 3

Fig. S3. Comparison of near-field and far-field spectra of BSA and γ-globulin. SINS imaginary spectra of BSA (red) and γ-globulin (blue) were recorded on dried proteins ∼240 nm and 400 nm thick, respectively. Far-field spectra (gray) were recorded with a thermal source in transmission and averaged over an area ∼60 × 60 μm^2.